JMEPEG (2006) 15:67-75
DOI: 10.1361/105994906X83501

1059-9495/$19.00

Influence of Thermal Exposure on the Microstructures and Mechanical Properties of a Superalloy

J.S. Hou and J.T. Guo

(Submitted July 31, 2005)

The effects of long-term aging on microstructures and their influence on tensile and stress-rupture behavior of a corrosion resistant nickel-base superalloy are investigated. Samples are aged isothermally at 1073, 1123, or 1173 K for different times of up to 10,000 h and mechanical tests are performed on samples in both standard heat treatment (SHT) and aged conditions. Scanning electron microscopy (SEM) studies reveal that the coarsening kinetics of γ' follows a linear law at different temperatures with the calculated activation energy, i.e., 255 kJ/mol, for γ' growth according to Lifshitz-Slyozof-Wagner (LSW) theory. After long-term aging for more than 1 khours, σ phase appears in the alloy. The kinetics of σ formation can be described by the Johnson-Avrime-Mehl equation. Tensile experiments at room temperature and 1173 K and endurance experiments at 1173 K/274 MPa are performed to test the effect of σ phases on these properties and no remarkable harmful effect is found. γ' coarsening can be used to explain the reduction of yield stress, which is tested by the Labusch-Schwarz hardening theory. Although the presence of the σ phase clearly does affect the fracture process, the σ phase does not embrittle the alloy.

Keywords mechanical properties, microstructure, nickel base superalloy, thermal exposure

1. Introduction

The experimental superalloy is a high-strength nickel-based superalloy that is being considered for application within modern gas turbine engines, e.g., in turbine blade applications. Its good mechanical properties at high temperatures are related to the structural hardening induced by precipitation of the ordered γ' phase. The strength of a given Ni-base superalloy is dependent upon such factors as volume fraction, size, and coarsening rate of γ' precipitates (Ref 1). Knowledge of the effects of service exposure on precipitate characteristics and related mechanical properties is an essential step in optimizing the properties of superalloys and prevent premature failure of components during service. For improving the high-temperature capability of these applications efficiency, recently developed alloys contain high amounts of refractory elements, such as Cr, W, and Mo, which act as solid solution strengtheners at high temperature (Ref 2). The introduction of these elements, however, makes the microstructure more susceptible to the formation of topologically closed packed (TCP) phases during long-term service (Ref 3, 4). Among these TCP phases, σ phase is a commonly observed phase in superalloys in which the total atomic percent of W and Mo is less than 3.8% (Ref 5). A great quantity of platelike structure is a critical property because it removes important strengthening refractory metal and chromium elements from the alloy matrix, causing loss of strength in the matrix (Ref 3, 6, 7). It is also reported that these brittle intermetallic TCP phases can initiate or accelerate crack propagation as they precipitate (Ref 8).

The experimental alloy, which consists of γ matrix, γ' precipitates, eutectic, carbides, and minor borides, is a cast nickel-based superalloy. To posses excellent hot-corrosion resistance and high-temperature oxidation resistance capability, the alloy contains 16% Cr and 10% Co (in wt.%). Furthermore, the target temperature capability of the alloy is set at 1373 K for 1000 h creep life. So the performance of the alloy after thermal exposure needs to be evaluated. This paper aims at: (a) coarsening behavior of γ' precipitates; (b) σ phase precipitation behavior; and (c) evaluating the effect of microstructure on the mechanical properties with identifying the governing mechanisms for the strength of the alloy, which will be helpful in future corrosion-resistant superalloy design.

2. Experimental

Experimental alloy was produced in an industrial scale vacuum induction furnace. Then 25 kg master ingot was remelted and cast into rods of 15 mm in diameter and 120 mm in length under vacuum. The chemical composition of the alloy (in wt.%) is about 15.5 Cr, 10.8 Co, 5.6 W, 2.1 Mo, 3.2 Al, 4.6 Ti, 0.2 Nb, 0.4 Hf, 0.075 B, 0.073 C, and the balance Ni. The specimens used for long-term aging were with the gauge section of diameter 15 mm and length 20 mm and were subjected to standard heat treatment (SHT), 1443 K/4 h/air cool + 1323 K/4 h/air cool + 1123 K/16 h/air cool. After standard heat treatment, the specimens were divided into several separate groups and some of the groups were given long-term, unstressed, high-temperature exposures at 1073, 1123, and 1173 K for 1000 h (1 kh), 3000 h (3 kh), 5000 h (5 kh), and 10,000 h (10 kh), respectively, to determine the microstructural evolution of the alloy.

J.S. Hou and **J.T. Guo,** Department of Superalloys, Institute of Metal Research, Chinese Academy of Sciences, Shenyang, P.R. China. Contact e-mail: jshou@imr.ac.cn.

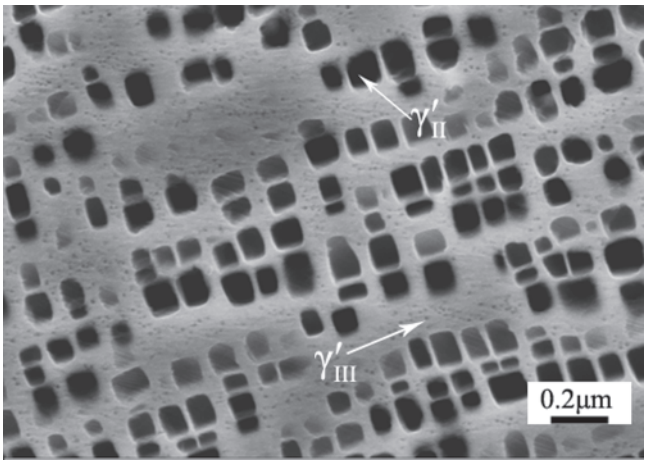

Fig. 1 SEM microstructure after standard heat treatment showing duplex size γ' distribution

Room and high-temperature tensile tests at initial strain rate from 1.04×10^{-4} to 1.04×10^{-1} s^{-1} were performed on a Shimadzu AG-250KNE test machine (Shimadzu Co., Ltd., Japan). The specimens for tensile tests were machined from the heat-treated bars, with the gauge section of diameter 5 mm and length 25 mm. The stress-rupture tests were conducted in air at 1173 K and 274 MPa. The transmission electron microscopy (TEM) foils were prepared by conventional jet polishing in a solution and finally observed in a Philips TEM 420 transmission electron microscope (Royal Dutch Philips Electronics Ltd., The Netherlands) operating at 100 kV. Metallography samples were examined on JSM-6301 scanning electron microscope (SEM) equipped with an energy-dispersive spectrometer (EDS) after being etched in Nimonic etching reagent (20 ml HCl, 5 g $CuSO_4$, and 80 ml H_2O). Quantitative measurements of σ and γ' precipitates were made directly on the SEM micrographs using a semiautomatic image analyzer. The reported values were the average values from the measurements made on ten SEM micrographs of each sample. The weight fraction of γ' was measured using the electrolytic extraction technique described by Kreige and Baris (Ref 9). The volume fraction of γ' was approximated to the weight fraction (Ref 11). In this study, the total volume fraction of γ' was almost constant during aging, i.e., ~51%.

3. Results and Discussion

3.1 Initial Microstructure

During solution treatment at 1443 K, almost all the γ' precipitates are dissolved except for the γ' particles (γ_I') in interdendritic regions and at the grain boundaries. After solid solu-

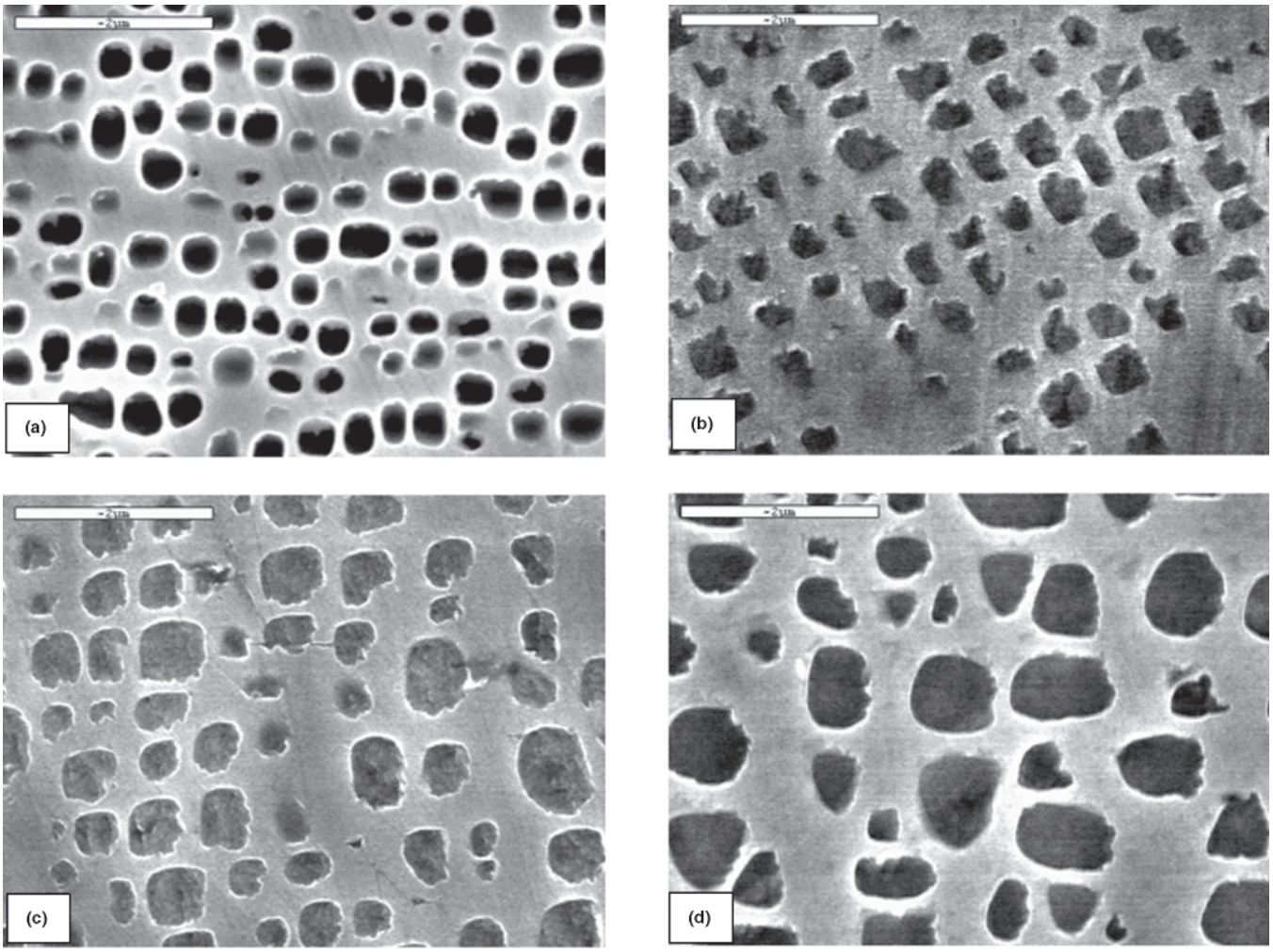

Fig. 2 γ' size and distribution after aging at 1123 K for (a) 1 kh, (b) 3 kh, (c) 5 kh, and (d) 10 kh

tion for 4 h followed by air cooling, in the dendritic cores the secondary γ' precipitate (γ_{II}') is cubic in mean edge length of 0.1 μm, while in interdendritic regions it is irregular. After further aging at 1323 K for 4 h followed by air cooling, the average edge length of γ_{II}' is about 0.12 μm due to reprecipitation. Then, after further aging at 1123 K followed by air cool, a duplex-size precipitate microstructure is obtained in dendritic cores, with the fine γ' particles called tertiary γ' precipitates (γ_{III}'). γ_{II}' and γ_{III}' particles in dendritic cores are cubic in mean edge length of 0.14 μm and spherical with a mean radius of 0.03 μm, respectively (Fig. 1).

3.2 Coarsening of γ' Precipitates

After aging treatment, the average γ' size increases with temperature increasing and also increases with aging time increasing. Figure 2(a-d) show the γ' coarsening at 1173 K for 1, 3, 5, and 10 kh, respectively. It is noted that some of the larger aged γ_{III}' are exhibited in these figures, and small ones cannot be seen with these experimental conditions. Subsequently, the study of γ' evolution is mainly on the γ_{II}' in dendritic cores. Although the larger secondary γ' precipitates present degenerate shape, the authors shall refer to them as cuboids. In this study, the average size of the degenerate cuboids is measured in terms of the diameter of a disc of equal projected area, so it is also considered as mean diameter of these cuboids. The average effective radius of γ' precipitates in this study with various aging times at three temperatures is plotted in Fig. 3(a). It is clear that the relationship between effective radius and aging time is linear (LSW theory) (Ref 10, 11):

$$\bar{d}^3 - \bar{d}_0^3 = kt \qquad \text{(Eq 1)}$$

where t is the aging time and $\bar{d}_0$ and $\bar{d}$ are the average size of γ' precipitates before aging and at the time t, respectively, which yields the coarsening rate, k. With assuming the composition of the γ' phase does not change significantly during isothermal aging, Steven and Flewitt (Ref 12) give the relation for calculating the activation energy for γ' coarsening, Q, as:

$$\ln(kT) = \text{constant} - Q/RT \qquad \text{(Eq 2)}$$

where T is the absolute temperature and R the gas constant. This relation is plotted in Fig. 3(b), which yields an active energy of 255 kJ/mol for γ' coarsening in the alloy. In Ni-based superalloys, estimated values of the activation energy for coarsening of γ' particles are approximately 250-290 kJ/mol, which are roughly consistent to that for diffusion of γ' formation elements in Ni (Ref 1). Therefore, the growth of γ' in these alloys is controlled mainly by the diffusion of Al, Ti, and Nb in the matrix. The γ' formation elements, such as Ni, Al, Ti, Nb, and W, diffuse from matrix to promote the γ' growth, with the interrelated diffusion of other elements (such as Co, Cr, and Mo) away from a coarsening γ' particle.

Mullins and Sekerka (Ref 13) proposed that the point effect of diffusion, which is the origin of morphological instability, competes with several stabilizing factors such as surface energy, surface diffusion, or anisotropy of surface tension (Ref 14). If the former is dominant, then instability occurs; if the latter factors are dominant, then the second phase grows without instability (Ref 14). As shown in Fig. 2, the mean size of γ' increases with increasing aging time, while the quantity of γ' decreases. It is clear to see that the cubic γ' particles degenerate and some relatively small γ' particles split (Fig. 2b, d). Two possible mechanisms could be deduced for the dissolution of coarser precipitates. One is the corner dissolution of coarse precipitates, which incorporates solute into the matrix solid solution. A second possible mechanism is a stepwise splitting of the coarser precipitates into smaller ones for the purpose of easier dissolution. Coarse precipitates usually split into two fractions and dissolution of the split portions occurs starting at the split plane (Ref 15). Thus, the degeneration of cubic γ' is due to the corner dissolution of γ' particles. However, the larger γ', which is dominated by total interface-related energy, will grow without instability, and the small cubic γ' particles, which will split and dissolve into supersaturated matrix, provide the solute for larger γ' growth.

3.3 σ Formation

With the aid of the d-electrons concept, the average d-orbital energy of the alloy is calculated as $\bar{M}_d = 0.986$, which is close to the upper bound of σ formation in high-strength nickel-based superalloys (0.975-0.991). By means of a

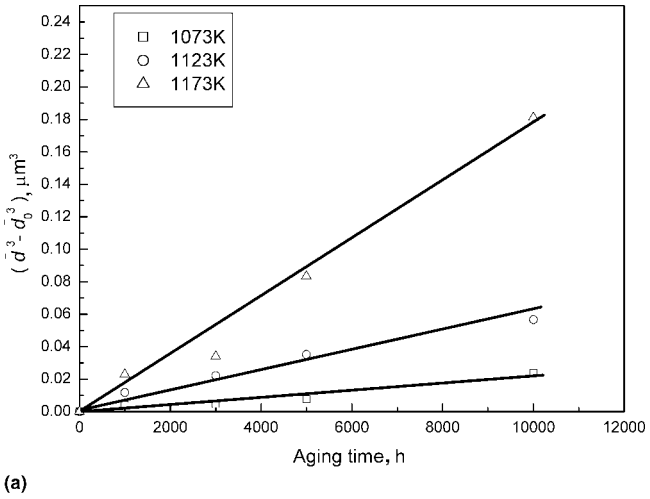

(a)

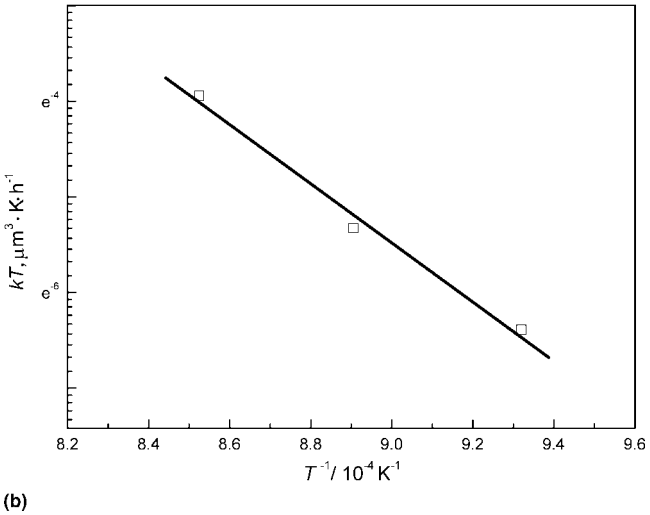

(b)

Fig. 3 Coarsening of γ' precipitates (a) correlation between ($\bar{d}^3 - \bar{d}_0^3$) and aging time at different temperature; (b) the relationship between temperature (T) and the growth rate (k) yielded from (a)

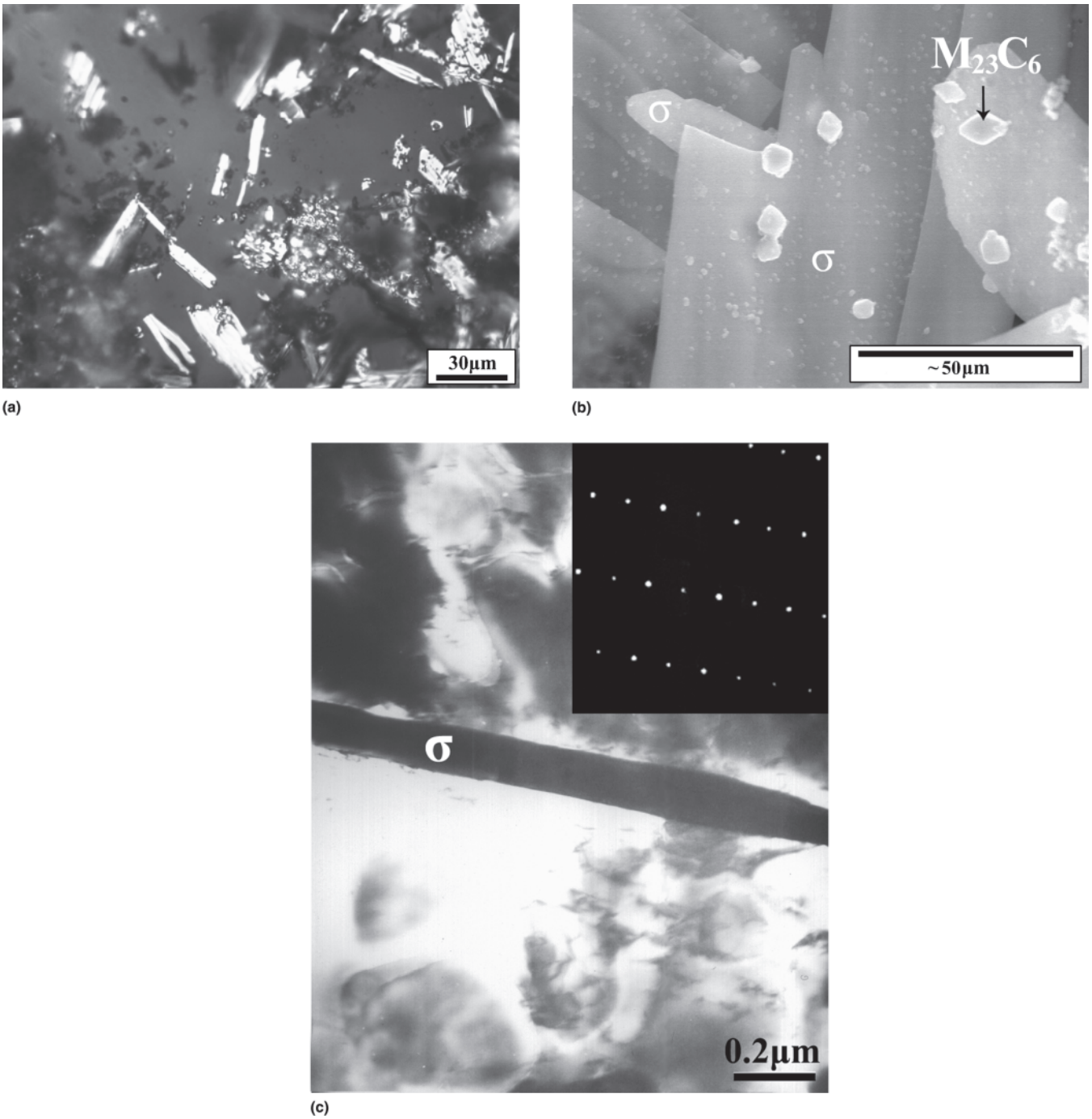

Fig. 4 Microstructure of the alloy after aging for 5 kh at 1123 K: (a) optical micrograph of σ plates extracted from alloy; (b) high magnified SEM micrograph of σ plate; and (c) TEM morphology of σ plate and corresponding diffraction pattern

phase computation (PHACOMP) method, the average electron-hole concentration (N_v) is calculated as $N_v = 2.475$, which is also close to the critical values for σ formation in superalloys (2.45-2.52). The higher value of $\overline{M}_d$ or N_v is due to the composition of the refractory elements in the alloy, which increases the tendency of TCP formation. The σ plates, which come from the sample aged for 5 kh at 1123 K with deep etching, are shown in Fig. 4(a). The extracted σ is in the form of thin rectangular plates, 20-50 μm long, 5-10 μm wide, and about 0.3 μm thick. The σ phase presents a lath-like character by high-magnification SEM study (Fig. 4b). TEM morphology of the σ plate with a corresponding diffraction pattern is shown in Fig. 4(c). After standard heat treatment and additional long-term isothermal aging at 1173 K for different times, σ phase formation occurs, as can be seen from Fig. 5. It is noticed that no σ phases are observed in the as-heat-treated samples or the samples exposed at 1173 K for 1 kh, but σ is being observed at longer exposure durations. As shown in Fig. 5(b) to (d), small blocky $M_{23}C_6$, which is enriched in Cr, precipitates within dendrite cores during aging heat treatment. Furthermore, the σ phase nucleates on $M_{23}C_6$ or in the vicinity of $M_{23}C_6$. The normalized volume fraction of σ phase, *f*, is derived from the

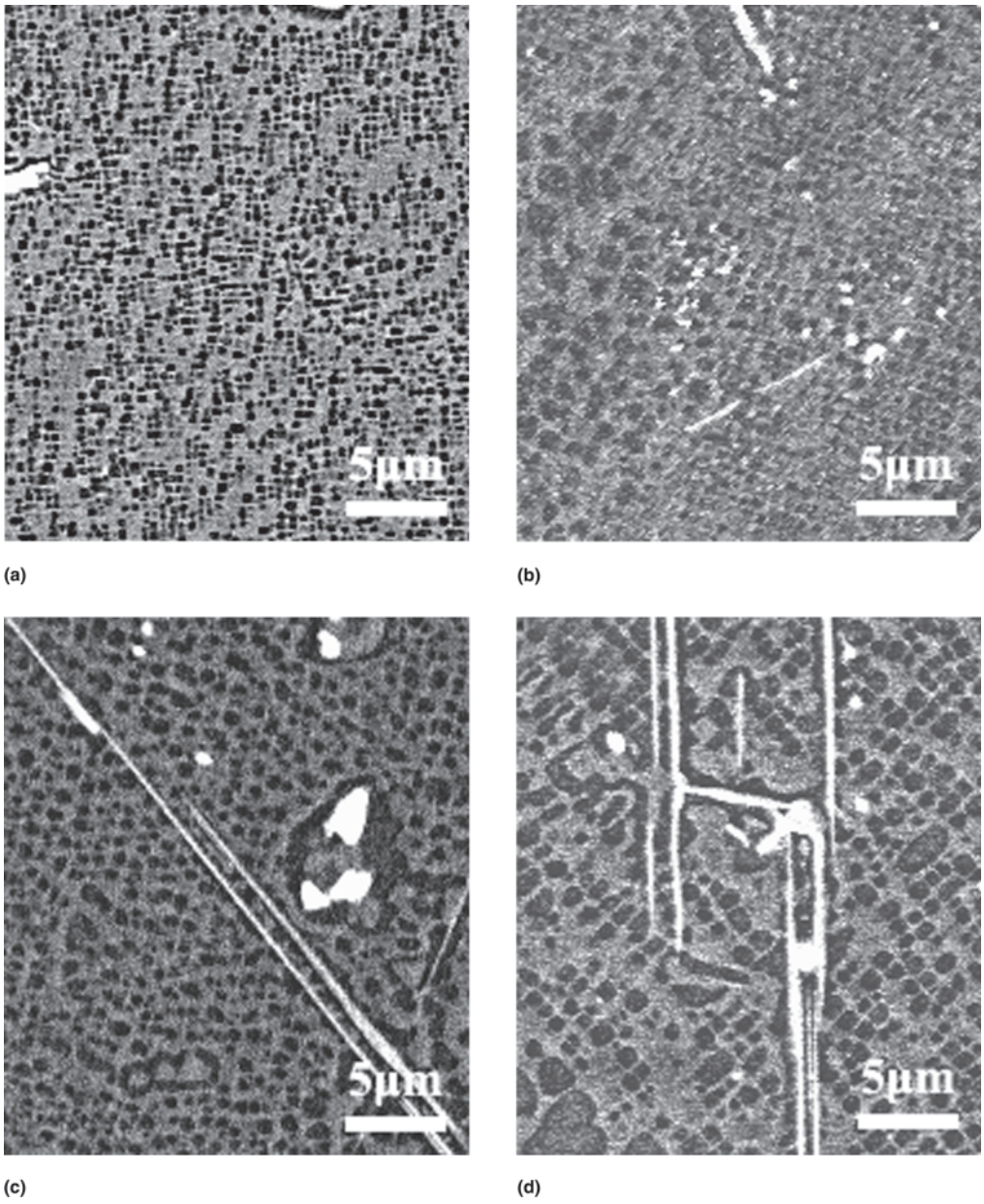

Fig. 5 Back-scattered electron micrographs depicting σ phase formation of samples aged at 1173 K for (a) 1 kh, (b) 3 kh, (c) 5 kh, and (d) 10 kh

area fraction of σ phase. The *f*-values versus aging time at different aging temperatures are displayed in Fig. 6. It shows that the incubation time for σ nucleation decreases and formation rate of σ increases with the aging temperature increasing. To better understand the fraction-increasing tendency of σ phase, the *f* data are fitted in terms of the Johnson-Avrami-Mehl (JAM) equation (Ref 16):

$$f = 1 - \exp(-kt^n) \quad \text{(Eq 3)}$$

where k is a constant, and *n* is the time exponent, referred to as the Avrami exponent, which often takes integer values of between 1 and 4. The various values of *n* are linked to factors such as shape, the nucleation or growth rate (Ref 17).

The best-fit values of the JAM equation are presented in Table 1. It shows that exponent *n* is nearly constant (1.35-1.52), so it is deduced that the nucleation mechanism of σ phase is not changed in the temperature range 1073-1173 K. On the basis of research of several alloys, Kim et al. (Ref 18) suggests that the growth of γ′ is controlled mainly by the bulk diffusion of Al or Ti in the matrix, with the interrelated diffusion of other γ′ formation elements (such as Co, Cr, and Mo) away from a growing γ′ particle. During the incubation of σ phase formation, which is the early stage of γ′ growth, the growth rate of γ′ is high. At this stage, the interface energy of γ/γ′ becomes low with elements diffusing rapidly, and the diffusion activation energies of these alloying elements become lower. Consequently, the σ formation elements are super saturation in matrix, and the concentration of these elements in the rich-W regions, the vicinity of $M_{23}C_6$, causing the preferential nucleation of σ phase. In the steady state of σ formation, the long-range diffusion of element Mo is the dominating factor to

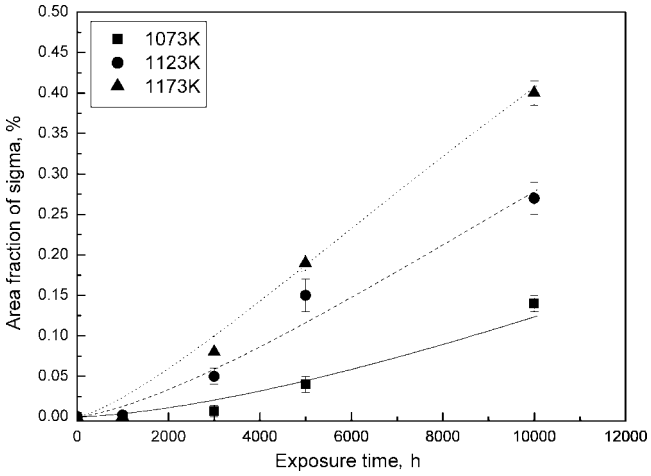

Fig. 6 Variations in σ phase fraction as a function of aging time and temperature

Table 1 Kinetics parameters *n* and *k* as obtained by fitting the data shown in Fig. 4 in terms of the JAM equation

Temperature, K	*n*	*k*, h^{-1}
1073	1.52	1.1×10^{-7}
1123	1.4	8.2×10^{-7}
1173	1.35	2.1×10^{-6}

control the σ growth (Ref 17). In the alloy, no obvious σ formation at grain boundaries can be attributed to the elements Hf and B, which concentrate or forms precipitates at grain boundaries; therefore, these elements adjust the distribution of carbides or prevent the MC from decomposing into $M_{23}C_6$ (Ref 19).

3.4 Mechanical Properties

The effect of aging time at different aging temperatures on yield stress and elongation of the alloy is presented in Fig. 7. It can be observed that the entire yield stresses decrease with aging time increasing. The amount of decrease in yield stress is drastic at the early stage of aging and small at the late stage of aging. Furthermore, the yield stress is higher at room temperature tests (Fig. 7a) than at 1173 K tests (Fig. 7b); thus it is independent of the aging temperature. The magnitude of the elongations fluctuates around that of the standard heat-treated samples, which is also independent of the aging temperature. Moreover, the elongations at RT tensile tests are lower than the tensile tests at 1173 K.

After thermal exposure at a temperature of 1173 K, the stress-rupture life is the longest (Fig. 8a). Furthermore, the reduction of endurance life becomes diminutive with aging time increasing. In addition, the endurance elongation of samples given long-term thermal exposures fluctuates around that of unexposed samples. It obtains the highest value after the samples are given long-term thermal exposure at 1173 K (Fig. 8b). These results are not consistent with the earlier polycrystalline Ni-base superalloys such as IN 100 (Ref 20) and U-700 (Ref 21) in which the long-term thermal exposures cause significant reduction effect on rupture strength accompanied by a reduction in rupture ductility.

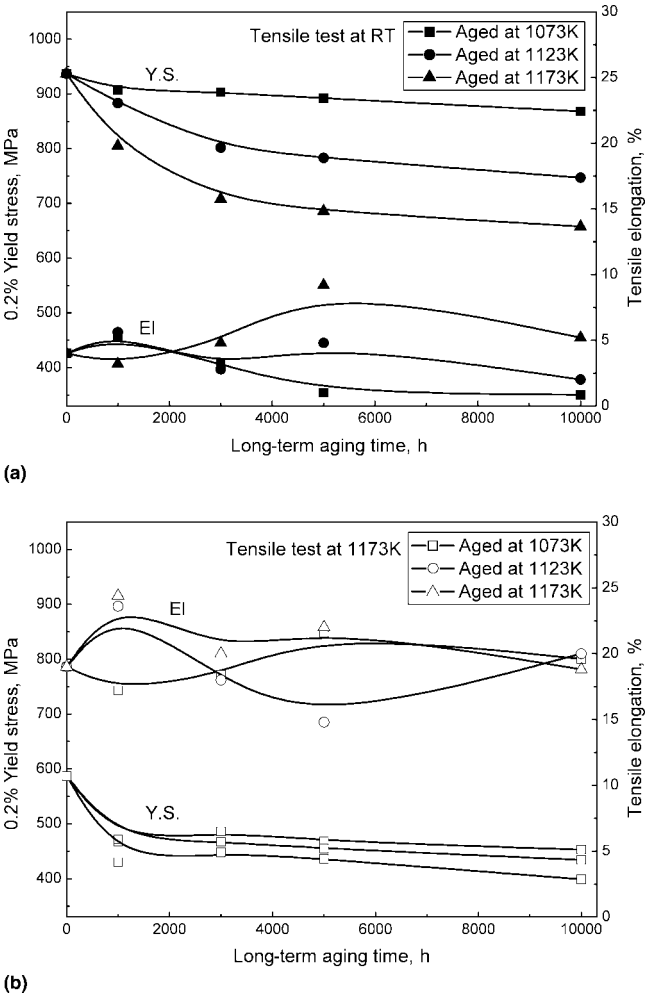

Fig. 7 Effect of aging time on tensile properties at (a) room temperature and (b) 1173 K

Discriminating the effect of phases such as γ′ and σ on the mechanical properties is really difficult because all of these phases are variable during long-term thermal exposure. It is well known that the σ phase has deleterious effects on mechanical properties in two different ways: the phase can act as a barrier for moving dislocations, leading to interfacial decohesion and crack initiation. Some researchers report that increased rupture ductility is considered to be mainly due to γ′ precipitate coarsening in alloys where no σ phase formation occurs (Ref 22, 23). Although the presence of σ phase is always reported to be related to embrittlement, which is considered to contribute to poor ductility (Ref 22), some researchers find that σ formation results in a decrease in the refractory metal content in the alloy matrix, causing a reduction in the strength and, perhaps, an increase in the ductility of the alloys (Ref 1, 3, 8). On the other hand, when σ phase is very little and small in quantity, it has no obvious effect on mechanical properties; furthermore, it can strengthen alloy at special conditions (Ref 24).

The SEM fractographic analysis of the samples after tensile test at 1173 K and stress-rupture test at 1173 K/274 MPa indicate that all samples fail in a ductile shear mode. It is found that, in long-term aged samples, σ phase presents a complicated fracture feature that occurs generally by the intergranular crack propagation method. In this case, the fracture presents

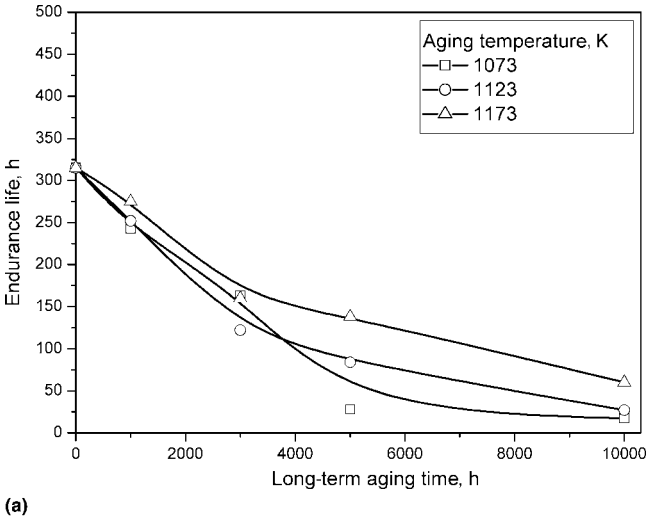

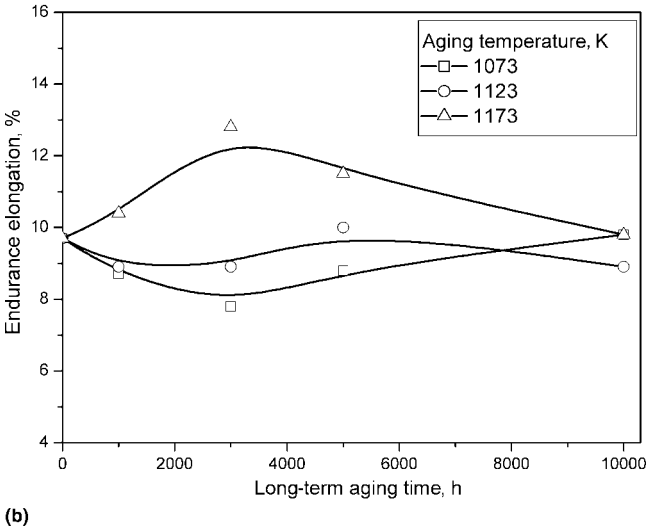

Fig. 8 Effect of aging time on stress-rupture properties at 1173 K with an engineering stress of 274 MPa: (a) stress-rupture life and (b) elongation

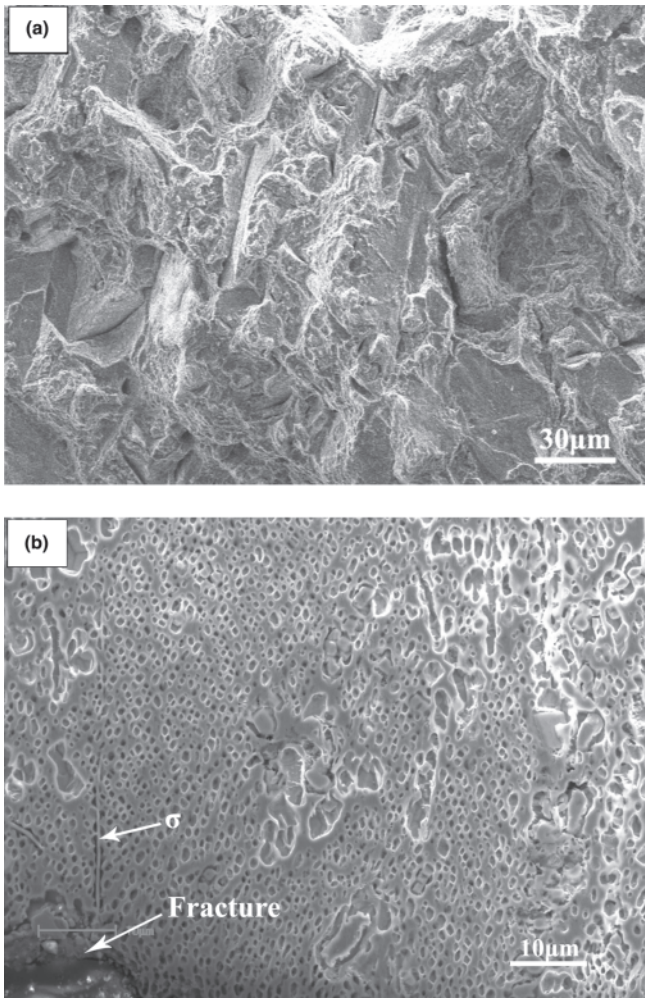

Fig. 9 SEM fractographies of (a) sample after 1123 K tensile test aged for 5 kh at 1123 K and (b) a longitudinal section of the sample after a stress-rupture test at 1173 K/274 MPa aged for 10 kh at 1173 K

mainly dimples with some facets that have similar dimensions with σ plates (Fig. 9a). Detailed study indicates that cracks initiate at interface of σ and γ/γ′ eutectic or carbide and matrix and advance across the grains leading to fluctuation of ductility (Fig. 9b). Therefore, samples with and without σ phases are not embrittled. Actually, it is believed that the growth of γ′ particles causes the variation of ductility, which also contributes to the reduction in endurance strength after the higher temperature exposure.

In high-strength materials, ordered secondary phase particles act as strong obstacles for moving dislocations in a disordered matrix. In this case, the conventional hardening theory, including pairwise particle cutting models proposed by Brown and Ham (Ref 25), Huther and Reppich (Ref 26), and the Orowan bowing model proposed by Brown and Ham (Ref 25), is normally used. In this study, models for Orowon bowing are not considered because Orowan loops are rarely seen in similar superalloys (Ref 23, 27, 28). Here, the Lbusch-Schwarz modified conventional hardening theory is used. Table 2 lists the appropriate formulas and the corresponding parameters used in this paper for estimating the CRSS in different rangers of par-

Table 2 Formulas and corresponding parameters used in this study

	CRSS for particle shearing	
Cutting stress for weakly coupled pairs	$\Delta\tau_0 = \frac{1}{2}\left(\frac{\gamma}{b}\right)^{3/2}\left(\frac{bdf}{\Gamma}\right)^{1/2} A - \frac{1}{2}\left(\frac{\gamma}{b}\right) f$	(Eq 4)
	$\Gamma \approx (Gb^2/2)/3.4; A = 0.72$	(Ref 27)
Cutting stress for strongly coupled pairs	$\Delta\tau_0 = \left(\frac{1}{2}\right) 1.72 \frac{\Gamma f^{1/2} w}{bd}\left(1.28 \frac{d\gamma}{w\Gamma} - 1\right)^{1/2}$	(Eq 5)
	$\Gamma \approx Gb^2/2$	(Ref 27)
Labusch-Schwarz correction for formulae (4) and (5)	$\Delta\tau_{LS} = 0.95(1 + C\eta_0)\Delta\tau_0$	(Eq 6)
	$\eta_0 \approx \eta_0^{min} = \sqrt{\frac{f}{\pi}}$	(Ref 27, 30)

Variables: γ, antiphase domain boundary (APB) energy; *b,* Burgers vector of the edge dislocation in matrix; *d,* mean particle diameter; *f,* volume fraction of γ′; Γ, dislocation line tension; *G,* shear modulus; *w,* constant

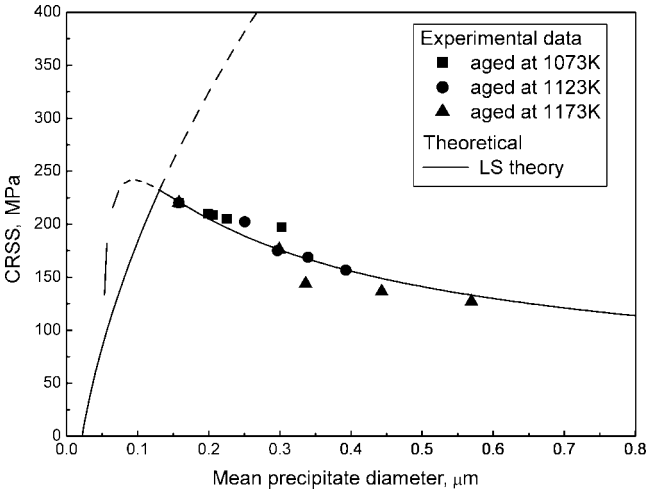

Fig. 10 Theoretical and measured critical resolved shear stress (CRSS) versus particle diameter

ticle diameters. In Eq 4 and 5, the dislocation line tensions Γ are described simply by the constant line tension approximation (Ref 27). In Eq 5, $w = 2.8$ for a volume fraction of 51%, is a constant that accounts for the elastic repulsion between the strongly paired dislocations. For larger γ' volume fraction, the Labusch-Schwarz model (Ref 29), which has been successfully applied to some Ni-base superalloys (Ref 27, 30), the appropriate interpolation formula, Eq 6, is valid, with $\Delta\tau_{LS}$ standing for the CRSS for the Labusch-Schwarz hardening model. As a simple approximation, the Labusch-Schwarz parameter (η_0) can be given as:

$$\eta_0^{\min} = \sqrt{\frac{f}{\pi}} \qquad \text{(Eq 7)}$$

This parameter is constant for a given f, independent of the particle size. In the calculation, the parameter η_0, i.e., $\eta_0^{\min} = 0.4$ ($f = 51\%$), is approximated. In Ni-base alloys, the total CRSS τ_0 includes the CRSS caused by solid solution hardening of the matrix τ_m, and the CRSS caused by γ' precipitates $\Delta\tau_0$. For simplification, the linear law $\tau_0 = \tau_m + \Delta\tau_0$ is applied in this study, and the value of τ_m is taken to be 92 MPa according to that of Nimonic 105, whose γ' volume fraction is also 51% (Ref 27). The yield stress σ_y has the relationship $\sigma_y = M\tau_0$, here the Taylor factor $M = 3$.

In the present study, the following values of parameters that are appropriate to the alloy have been assumed: $b = 0.254$ nm, $\gamma = 0.12$ J/m^2, $f = 0.51$, $G = 80$ GPa (298 K) or 56 GPa (1173 K). The CRSS $\Delta\tau_0$ due to γ' particles as a function of mean particle diameter d, in which the experimental data associate with the theoretical curve, is shown in Fig. 10. Good agreement is observed between experimental data and LS theory values (thick full lines), and the transition from shearing to Orowan mechanism is observed to occur at the mean diameter of about 0.5 μm. Furthermore, it derives the diameter of $d = 0.13$ μm, when transition from weak-coupled pairs dislocation shearing to strong-coupled pairs dislocation shearing occurs. As anticipated, the yield stress at 1173 K for the aged alloy is lower than at room temperature. With the LS theory, the weak-strong coupled pairs transition diameter is calculated also to be about 0.13 μm.

From graphs such as Fig. 10, it is concluded that the strength reduction can be explained by γ' coarsening. So it also gives evidence that σ phase cannot influence the strength obviously. σ phase formation in the alloy is mainly in dendrite cores with a few at interdendritic regions other than in the vicinity of grain boundaries in early reported superalloys such as IN100 (Ref 20) and U720 (Ref 31). This character of σ phase reduces the risk of rapid grain boundary crack propagation. Moreover, the number of σ is not large and their distribution is not wide enough to make the σ phases conjoin in the alloy, avoiding the penetrating crack. So no remarkable harmful effect on the mechanical properties can be found. Although the presence of the σ phase clearly does affect the fracture process, the σ phase does not embrittle the alloy.

4. Conclusions

- Coarsening kinetics of γ' precipitates in the alloy follows a linear law at different temperatures. Calculated with the LSW theory, the activation energy for the growth of γ' precipitates, i.e., about 255 kJ/mol, is close to the activation energies for diffusion of γ' formation elements in nickel.
- After long-term exposure, there are small amounts of σ phases that appear in the alloy. From JAM theory analysis, the exponent n is nearly constant (1.35-1.52). The σ formation mechanism is suggested as the diffusion of σ formation elements.
- In the alloy, σ phases influence the mechanical properties mainly by softening of the γ matrix rather than by embrittlement, which is verified by no drop in ductility. The degeneration of strength is mainly due to the coarsening of γ' precipitates. With Lbusch-Schwarz theory, the predicted precipitate diameter corresponding to peak strengthening is about 0.13 μm.

References

1. A. Baldan, Progress in Ostwald Ripening Theories and Their Application to the γ' precipitates in Ni-base superalloys, *J. Mater. Sci.,* 2002, 37, p 2379-2405
2. E. Lvova and D. Norsworthy, Influence of Service-Induced Microstructural Changers on the Aging Kinetics of Rejuvenated Ni-Based Superalloy Gas Turbine Blades, *J. Mater. Eng. Perf.,* 2001, 10, p 299-313
3. R. Darolia, D.F. Lahrmann, R.D. Field, and R. Sisson, Directionally Solidified/Single Crystal Alloys, *Superalloys 1988,* S. Reichmann, D.N. Duhl, G. Maurer, S. Antolovich and C. Lund, Ed., TMS, 1988, p 255
4. G.L. Erickson, Alloy Development, *Superalloys 1996,* R.D. Kissinger, D.J. Deye, D.L. Anton, A.D. Cetel, M.V. Nathal, T.M. Pollock, and D.A. Woodford, Ed., TMS, 1996, p 35
5. R.F. Decker and C.T. Sims, *The Superalloys,* C.T. Sims, W.C. Hagel Eds., John Wiley & Sons, Inc., New York, 1972, p 60
6. W. Scott Walston, *Long-Term Stability of High Temperature Materials,* G.E. Fuchs, K.A. Dannemann, and T.A. Deragon, Ed., TMS, 1999, p 43
7. M. Morinaga, N. Yukawa, H. Ezaki, and H. Adachi, New PHACOMP and Its Applications to Alloy Design, *Phil. Mag. A,* 1985, 51, p 223-247
8. S. Tin and T.M. Pollock, Phase Instabilities and Carbon Additions in Single-Crystal Nickel-Base Superalloys, *Mater. Sci. Eng. A,* 2003, 348, p 111-121
9. O.H. Kreige and J.M. Baris, The Chemical Partitioning of Elements in γ' Separated from Precipitation-Hardened High Temperature Nickel Base Alloy, *Trans. ASM,* 1969, 62, p 195-201

10. A.J. Ardell, The Effect of Volume Fraction on Particle Coarsening: Theoretical Considerations, *Acta Metall.,* 1972, 20, p 61-71
11. M. Doi, Coarsening Behaviour of Coherent Precipitates in Elastically Constrained Systems-With Particular Emphasis on γ′ Precipitates in Nickel-Base Alloys, *Mater. Trans. JIM,* 1992, 33, p 637-649
12. R.A. Stevens and P.E.J. Flewitt, The Effects of γ′ Precipitate Coarsening During Isothermal Aging and Creep of the Nickel-Base Superalloy IN-738, *Mater. Sci. Eng.,* 1972, 37, p 237-247
13. W.W. Mullins and R.F. Sekerka, Morphological Stability of a Particle Growing by Diffusion or Heat Flow, *J. Appl. Phys.,* 1963, 34, p 323-329
14. Y.S. Yoo, Morphological Stability of Spherical γ′ Precipitates in a Nickel Base Superalloy, *Scr. Mater.,* 2005, 53, p 81-85
15. E. Balikci and A. Raman, Characteristics of the γ′ Precipitates at High Temperatures in Ni-Base Polycrystalline Superalloy IN738LC, *J. Mater. Sci.,* 2000, 35, p 3593-3597
16. W. Sha, Computer Modeling of Isothermal Crystallization Kinetics of Electroless and Melt Quenched Amorphous Solids Using Johnson-Mehl-Avrami Theory, *Mater. Sci. Technol.,* 2005, 21, p 69-75
17. Y.S. Na, N.K. Park, and R.C. Reed, σ Morphology and Precipitation Mechanism in Udimet 720li, *Scr. Mater.,* 2000, 43, p 585-590
18. H.T. Kim, S.S. Chun, X.X. Yao, Y. Fang, and J. Choi, γ′ Precipitating and Ageing Behaviours in Two Newly Developed Nickel-Base Superalloys, *J. Mater. Sci.,* 1997, 32, p 4917-4923
19. R.F. Decker and J.W. Freeman, The Mechanism of Beneficial Effects of Boron and Zirconium on Creep Properties of a Complex Heat-Resistant Alloy, *Trans. AIME,* 1960, 218, p 277-283
20. R.L. Dreshfield and R.L. Ashbrook, NASA TN D-5158 (1969); NASA TN D-6015 (1970)
21. C.T. Sims, The Occurrence of Topologically Close Packed Phases, *The Superalloys,* C.T. Sims and W.C. Hagel, Ed., John Wiley & Sons, Inc., New York, 1972, p 260
22. S.T. Wlodek, Keynote Address, *Long-Term Stability of High-Temperature Materials,* G.E. Fuchs, K.A. Dannemann, and T.A. Deragon, Ed., TMS, 1999, p 3
23. R. Sharghi-Moshtaghin and S. Asgari, The Influence of Thermal Exposure on the γ′ Precipitates Characteristics and Tensile Behavior of Superalloy IN-738LC, *J. Mater. Proc. Technol.,* 2004, 147, p 343-350
24. J.T. Guo, Application of Electron Hole Theory in Superalloys, *Physics,* 1982, 11, p 661-665, in Chinese
25. L.M. Brown and R.K. Ham, Dislocation-Particle Interactions, *Strengthening Methods in Crystals,* A. Kelly and R.B. Nicholson, Ed., Elsevier, Amsterdam, 1971, p 9-12
26. W. Huther and B. Reppich, Interaction of Dislocations With Coherent, Stress-Free, Ordered Particles, *Z. Metallkd.,* 1978, 69, p 628-634
27. B. Reppich, P. Schepp, and G. Wehner, Some New Aspects Concerning Particle Hardening Mechanism in γ′ Precipitating Nickel-Base Alloys, *Acta Metall.,* 1982, 30, p 95-104
28. M.P. Jackson and R.C. Reed, Heat Treatment of Udimet 720Li: The Effect of Microstructure on Properties, *Mater. Sci. Eng. A,* 1999, 259, p 85-97
29. R. Labusch and R.B. Schwarz, Dynamic Simulation of Solution Hardening, *J. Appl. Phys.,* 1978, 49, p 5174-5187
30. C. Yuan, J.T. Guo, H.C. Yang, and S.H. Wang, Deformation Mechanism for High Temperature Creep of a Directionally Solidified Nickel-Base Superalloys, *Scr. Mater.,* 1998, 39, p 991-997
31. D.J. Bryant and G. McIntosh, Powder Metallurgy and Wrought Materials, *Superalloys 1996,* R.D. Kissinger, D.J. Deye, D.L. Anton, A.D. Cetel, M.V. Nathal, T.M. Pollock, and D.A. Woodford, Ed., TMS, 1996, p 713